Title
The roles of changes in deoxyhemoglobin concentration and regional cerebral blood volume in the fMRI BOLD signal

Journal
NeuroImage, 19(4)

ISSN
1053-8119

Authors
Toronov, Vlad
Walker, Scott
Gupta, Rajarsi
et al.

Publication Date
2003-08-01

DOI
10.1016/s1053-8119(03)00152-6

ACADEMIC PRESS

Available online at www.sciencedirect.com
SCIENCE DIRECT®

NeuroImage

NeuroImage 19 (2003) 1521–1531

www.elsevier.com/locate/ynimg

The roles of changes in deoxyhemoglobin concentration and regional cerebral blood volume in the fMRI BOLD signal

Vlad Toronov,[a,*] Scott Walker,[a] Rajarsi Gupta,[b] Jee H. Choi,[b] Enrico Gratton,[b] Dennis Hueber,[c] and Andrew Webb[a]

[a] *Beckman Institute for Advanced Science and Technology, University of Illinois at Urbana-Champaign, 405 N. Mathews Avenue, Urbana, IL 61801, USA*
[b] *Laboratory for Fluorescence Dynamics, Department of Physics, University of Illinois at Urbana-Champaign, 1110 W. Green Street, Urbana, IL 61801, USA*
[c] *ISS Incorporated, 1602 Newton Drive, Champaign, IL 61822, USA*

Received 12 September 2002; revised 12 January 2003; accepted 3 March 2003

Abstract

To study the behavior of cerebral physiological parameters and to further the understanding of the functional magnetic resonance imaging (fMRI) blood-oxygen-level-dependent (BOLD) effect, multisource frequency-domain near-infrared and BOLD fMRI signals were recorded simultaneously during motor functional activation in humans. From the near-infrared data information was obtained on the changes in cerebral blood volume and oxygenation. To relate our observations to changes in cerebral blood flow the well-known "balloon" model was employed. Our data showed that the deoxyhemoglobin concentration is the major factor determining the time course of the BOLD signal. The increase in cerebral blood oxygenation during functional activation is due to an increase in the velocity of blood flow, and occurs without significant swelling of the blood vessels.

Introduction

One of the most basic questions in functional brain mapping is the hemodynamic mechanism of the oxygen supply to cortical tissue during neural activation (Bandettini et al., 1997; Buxton and Frank, 1997). Many studies have focused on assessment of the roles of various parameters characterizing this mechanism (Vanzetta and Grinvald, 1999; Ugurbil et al., 2000; Fox et al., 1986; Belliveau et al., 1991; Buxton et al., 1998; Feng et al., 2001; Hess et al., 2000). The problem, however, is that the output signals of most measurement techniques depend upon many different interrelated parameters. For this reason, the behavior of such important cerebral parameters as regional cerebral blood flow (rCBF), volume (rCBV), oxygenation (rCBO), and cerebral oxygen metabolic rate ($CMRO_2$) during cerebral activation remains controversial. In one study (Bandettini et al., 1997) the authors concluded that both rCBF and $CMRO_2$ remain constant during cortical activation, while other groups have reported significant changes in these parameters (Buxton et al., 1998; Feng et al., 2001; Hess et al., 2000). The basic idea of our work is to approach the problem by using two different measurement techniques, functional magnetic resonance imaging (fMRI) and near-infrared spectroscopy (NIRS).

The main advantages of fMRI in brain mapping studies are high spatial resolution and the absence of any penetration limits. However, the blood-oxygen-level-dependent (BOLD) effect is a complex biophysical phenomenon (Buxton et al., 1998; Boxerman et al., 1995; Ogawa et al., 1993). Buxton et al. (1998) recently proposed the following model of the BOLD signal:

$$\frac{S - S_0}{S_0} = V_0\left[k_1(1 - q) - k_2 v\left(\frac{q}{v} - 1\right) + k_3(1 - v)\right] \quad (1)$$

* Corresponding author. Fax: +1-217-244-6633.
E-mail address: toronov@uiuc.edu (V. Toronov).

1053-8119/03/$ – see front matter © 2003 Elsevier Science (USA). All rights reserved.
doi:10.1016/S1053-8119(03)00152-6

where S is the BOLD signal intensity from a particular "activated" voxel, Q is the deoxyhemoglobin content, V is the rCBV, the subscript 0 indicates the respective values at rest, $q = Q/Q_0$, and $v = V/V_0$. The dimensionless parameters k_1, k_2, and k_3 are positive and depend on the echo time TE, the oxygen extraction factor at rest E_0, the susceptibility difference between intravascular and extravascular medium at rest, and the ratio of intravascular and extravascular signals. The model implies that an increase in the BOLD signal can be caused both by a decrease in deoxyhemoglobin content and by an increase in rCBV.

In recent years many NIRS studies have demonstrated that cerebral hemodynamic changes associated with functional brain activity can be assessed noninvasively in adult human subjects (Benaron and Stevenson, 1994; Obrig et al., 2000). Several types of brain activity have been studied, including motor activity (Hirth et al., 1997; Colier et al., 1999; Toronov et al., 2000, 2001; Franceschini et al., 2000), visual activation (Ruben et al., 1997; Kato et al., 1993), auditory stimulation (Sakatani et al., 1999), and the performance of different cognitive tasks (Chance et al., 1993; Villringer et al., 1993). Kleinschmidt et al. (1996) were first to measure simultaneously the BOLD fMRI signal and hemoglobin changes using NIRS. Our group then reported the first NIR mapping of functional hemodynamics in human motor cortex with simultaneous fMRI measurements (Toronov et al., 2001). Although NIRS cannot compete with fMRI in terms of spatial resolution, the unique biochemical specificity of NIRS makes it a perfect complementary method to resolve difficulties in the physiological interpretation of the BOLD signal (Villringer and Chance, 1997). Particularly, using light sources at two different near-infrared wavelengths one can measure independently tissue oxy- and deoxyhemoglobin concentrations (Fantini et al., 1995). Therefore, using NIRS data acquired simultaneously with BOLD fMRI, one can directly assess the role of the two major physiological parameters underlying the BOLD signal, namely the rCBO and rCBV.

NIRS data can also be used to obtain changes in the rCBF and $CMRO_2$ by employing the "balloon" model (Buxton et al., 1998). The model is represented by a system of the following two differential equations:

$$\frac{dq}{dt} = \frac{1}{\tau_0}\left[f_{in}(t)\frac{E}{E_0} - f_{out}(t)\frac{q(t)}{v(t)}\right] \tag{2}$$

$$\frac{dv}{dt} = \frac{1}{\tau_0}[\, f_{in}(t) - f_{out}(t)] \tag{3}$$

where f_{in} and f_{out} are the input and output rCBF normalized to the baseline value of rCBF F_0, E is the oxygen extraction fraction (OEF), and the time constant τ_0 equals F_0/V_0. As shown in the study by Buxton and Frank (1997), the OEF can be expressed as a function of f_{in} by using the equation

$$E(f_{in}) = 1 - (1 - E_0)^{1/f_{in}} \tag{4}$$

Authors of the studies by Buxton et al. (1998) and Feng et al. (2001) used the "balloon" model to connect the BOLD fMRI signal with the rCBF measured by using an arterial spin-labeling (ASL) technique. A weakness of this approach is that it provides a rough estimate of only one variable, rCBF, in the balloon model. Both groups identified the measured rCBF with the variable f_{in}, and modeled f_{out} as a polynomial function of v, assuming significant (up to 30%) changes in the rCBV. Using NIRS, one can directly test the correctness of this latter assumption. Furthermore, applying Eqs. (2)–(4) to NIRS data, one can obtain independently the values of both f_{in} and f_{out}. Since the $CMRO_2$ is proportional to the product of the rCBF and OEF, which can be obtained using Eq. (4), NIRS also allows assessment of the time course of the $CMRO_2$.

The particular aims of our study were to directly assess the contributions of changes in the deoxyhemoglobin concentration and rCBV to the BOLD signal during cerebral activation in humans, and to investigate the temporal behavior of the rCBF, rCBV, rCBO, and $CMRO_2$. To achieve these aims echo-planar images (EPI) at 1.5 T and frequency-domain near-infrared signals were recorded simultaneously during motor activation.

All previous NIRS measurements of cerebral hemodynamics have been performed by using a single source-detector pair (see, for example, Toronov et al., 2001). In this study the optical properties of tissue were obtained from the slopes of the modulation amplitude (AC) and phase of the harmonically modulated optical signals measured at several source-detector distances (Fantini et al., 1995). This multichannel method allowed us (1) to measure not only changes in oxy- and deoxyhemoglobin concentrations, but also their baseline values, which are necessary for obtaining the parameters q and v in Eqs. (1)–(3); (2) to significantly reduce the effect of hemodynamic fluctuations in superficial tissues near the sources and detectors on the measured signals, and (3) to eliminate the crosstalk between light absorption and scattering (see experimental procedures section).

To clarify how cerebral oxy- and deoxyhemoglobin concentrations (denoted as $[O_2Hb]$ and [HHb], respectively) obtained from NIRS data can be applied to Eqs. (1)–(4), let us note that the variables q and v can be related to [HHb] and $[O_2Hb]$ as $q(t) = 1 - ([HHb]_0 - [HHb])/[HHb]_0$ and $v(t) = ([t\mathrm{Hb}] - [t\mathrm{Hb}]_0)/[t\mathrm{Hb}]_0$. It is assumed here that the total deoxyhemoglobin content Q within a voxel is equal to [HHb] multiplied by the voxel volume, and that, at a constant hematocrit, the blood volume fraction is proportional to the total hemoglobin concentration [tHb], which is the sum of [HHb] and $[O_2Hb]$. Changes in [tHb] have been demonstrated to be an accurate measure of changes in rCBV during functional activation (Ferrari et al., 1986, 1987, 1992). This agrees with the known fact that under normal conditions in healthy subjects the ratio of the [tHb] to rCBV (the hematocrit) does not change significantly during short periods of time such as the duration of typical functional

activation experiments. Then Eq. (1) can be rewritten in terms of hemodynamic concentration changes as

$$\frac{S(t) - S_0}{S_0} = A_P P(t) + A_R R(t) \quad (5)$$

where $P(t) = 1 - q(t)$, $R(t) = v(t) - 1$, $A_P = V_0(k_1 + k_2)$, and $A_R = V_0(k_2 + k_3)$. The coefficients A_P and A_R can be obtained from a bivariate regression analysis of the BOLD signal with $P(t)$ and $R(t)$ as the regressors. One can also obtain the flow parameters f_{in} and f_{out} in the balloon model by substituting $q(t) = 1 - P(t)$ and $v(t) = 1 + R(t)$ into Eqs. (2) and (3) and then by solving for f_{in} and f_{out}.

Materials and methods

Experimental equipment and procedures

MRI was performed by using a 1.5-T whole body MR scanner (Signa, General Electric Medical Systems, Milwaukee, WI) equipped with echo-speed gradients and a standard circularly polarized birdcage head coil. Sagittal T_1-weighted localizer scans were used to determine the correct plane for the functional scans. Gradient-echo echo-planar images were acquired by using a data matrix of 64 × 64 complex points, TR = 1280 ms, TE = 40 ms, FOV = 240 mm, slice thickness = 7 mm no interslice gap, receiver bandwidth 62.5 kHz, and flip angle 60°. The voxel size was 3.75 × 3.75 × 7 mm^3. Multimodality radiological markers (IZI Medical Products Corp, Baltimore, MD) were embedded into the optical sensor to facilitate correct orientation of the MRI slices with respect to the sensor and to enable recovery of the sensor orientation for data analysis.

For NIRS measurements a frequency-domain (110 MHz modulation frequency) Oximeter (ISS, Champaign, IL) was used, which had laser diode sources at wavelengths of 758 and 830 nm, and a photomultiplier tube detector. At a wavelength of 758 nm, light absorption by deoxyhemoglobin (HHb) substantially exceeds absorption by oxyhemoglobin (O_2Hb), while at 830 nm the O_2Hb absorption is much higher than the HHb absorption. The laser diodes operate in a sequential multiplexing mode. The whole acquisition cycle for 16 light sources was 160 ms. Light emitted by the laser diodes was guided to the tissue through 10-m-long multimode silica optical fibers (CUDA, Jacksonville, FL). Two 10-m-long glass-fiber bundles collected the scattered light and guided it to the detectors.

The optical sensor used in this study is shown in Fig. 1. The sensor had a detector, marked as *D*, and 12 paired light sources at six locations marked by numbers 1 through 6 (758 and 830 nm wavelengths at each location). The distances between the sources and detector were 2.5, 3.0, and 3.6 cm.

One possible source of signal distortions is the "crosstalk" between the absorption and scattering coefficients of tissue. If functional changes in the rCBV result in an increased number of red blood cells, the scattering coefficient of brain tissue would change between the activated and resting states. These scattering changes affect the measured DC, AC, and phase of the received optical signal. If one uses only the DC or AC part of the optical signal, i.e., one does not separate absorption from scattering, the measured changes are solely attributed to the absorption coefficient, which causes signal biasing. In contrast, our approach of using frequency-domain instrumentation together with a multichannel approach allows complete separation of absorption from scattering (Fantini et al., 1995).

One should note that the multichannel approach requires calibration of the optical sensor, which includes determination of the correction amplitude factors and phase terms from measurements of a calibration phantom with known optical properties (Fantini et al., 1995). These values are then used to calibrate the data obtained by using the same sensor in vivo. A silicone calibration block (ISS) was used, with optical properties at 758 and 830 nm close to those of the adult head: $\mu_a(758) = 0.107\ cm^{-1}$; $\mu_a(830) = 0.104\ cm^{-1}$; $\mu_s'(758) = 7.4\ cm^{-1}$; $\mu_s'(830) = 6.9\ cm^{-1}$, where μ_a is the absorption coefficient and μ_s the reduced scattering coefficient.

Calibration could be subject to errors due to the differences in the optical coupling between the light sources and detectors with the head. In particular, hair alters the coupling of the light sources and detectors with the skin in an irregular way. The other problem associated with hair is that it causes significant attenuation of light, which results in a low signal-to-noise (S/N) ratio of the phase of the modulated light signals. It was found that even the roots of shaved dark hair may attenuate the light to such an extent that the measurements using phase are strongly compromised. Therefore, for this study, naturally hairless subjects were selected. The optical sensor was centered at the measured C3 position of the left hemisphere. In cases when the analysis of the fMRI data revealed poor collocation between the activation focus and the optical sensor, the experiments were repeated with the optical sensor attached over the activation focus found during the previous measurement.

Each experiment comprised ten 10-s stimulation epochs, which were separated by ten 17-s control epochs. During stimulation epochs, subjects performed light palm squeezing with the right hand. Synchronization of the exercise sequence with the MRI and NIRS recordings was performed by a computer program that generated the commands for the subject and the scanner operator based on preset command timing. The total length of one data record was about 5 min.

Signal Processing

To determine whether the optical sensor was located close to the region of cerebral activation, fMRI statistical maps showing "activated regions" were obtained by using a *t* test of the EPI intensity variations between stimulation and rest. The activated voxels were determined as those showing

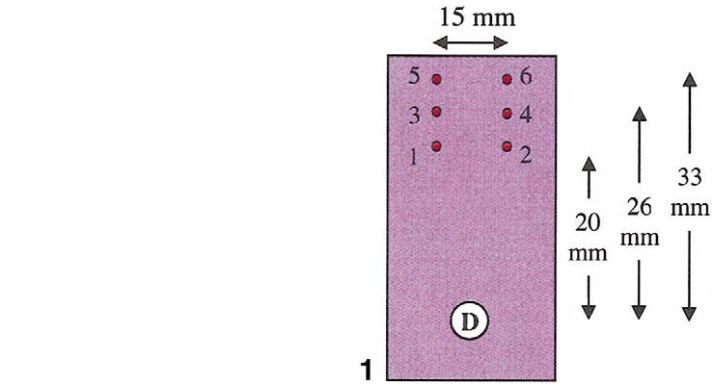

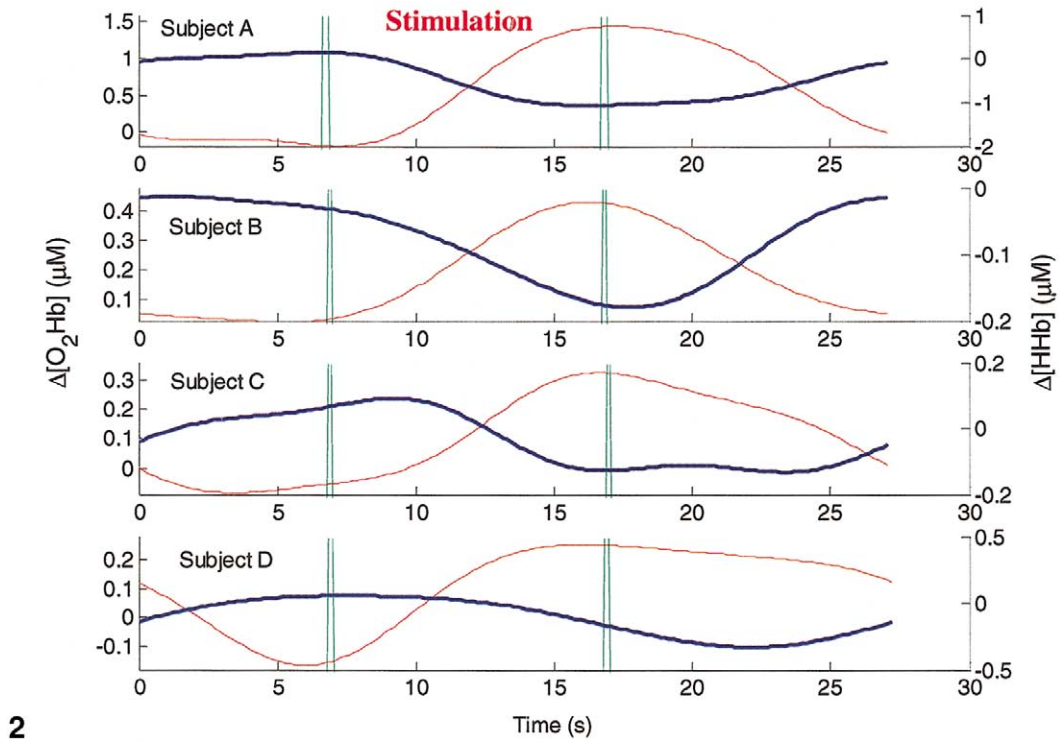

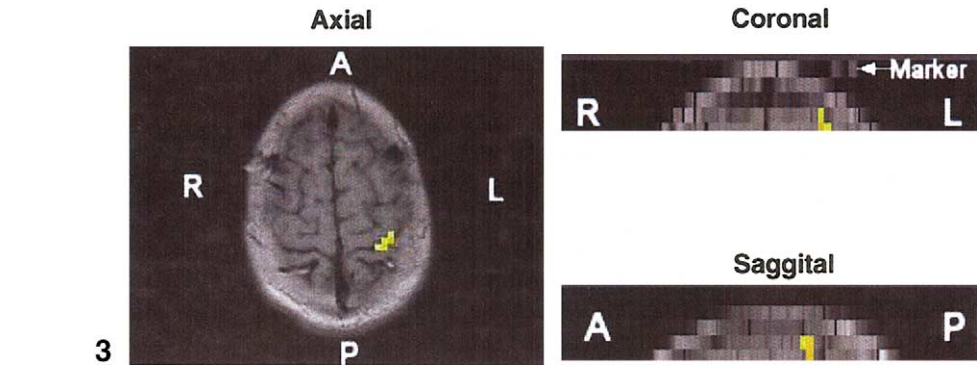

Fig. 1. The optical sensor. At each location marked by numbers 1–6 there were two light sources, at 830 nm and 758 nm.

Fig. 2. Changes in cerebral [O_2Hb] (hairlines) and [HHb] (bold lines) for each of four volunteers. Vertical marks indicate the beginning and the end of stimulation.

Fig. 3. A typical *F*-statistic map for the regression of BOLD signal with respect to $P(t)$ and $R(t)$. Activated voxels are shown in yellow. The letters A, P, R, and L show the image orientation according to radiological convention, and denote anterior, posterior, right, and left, respectively.

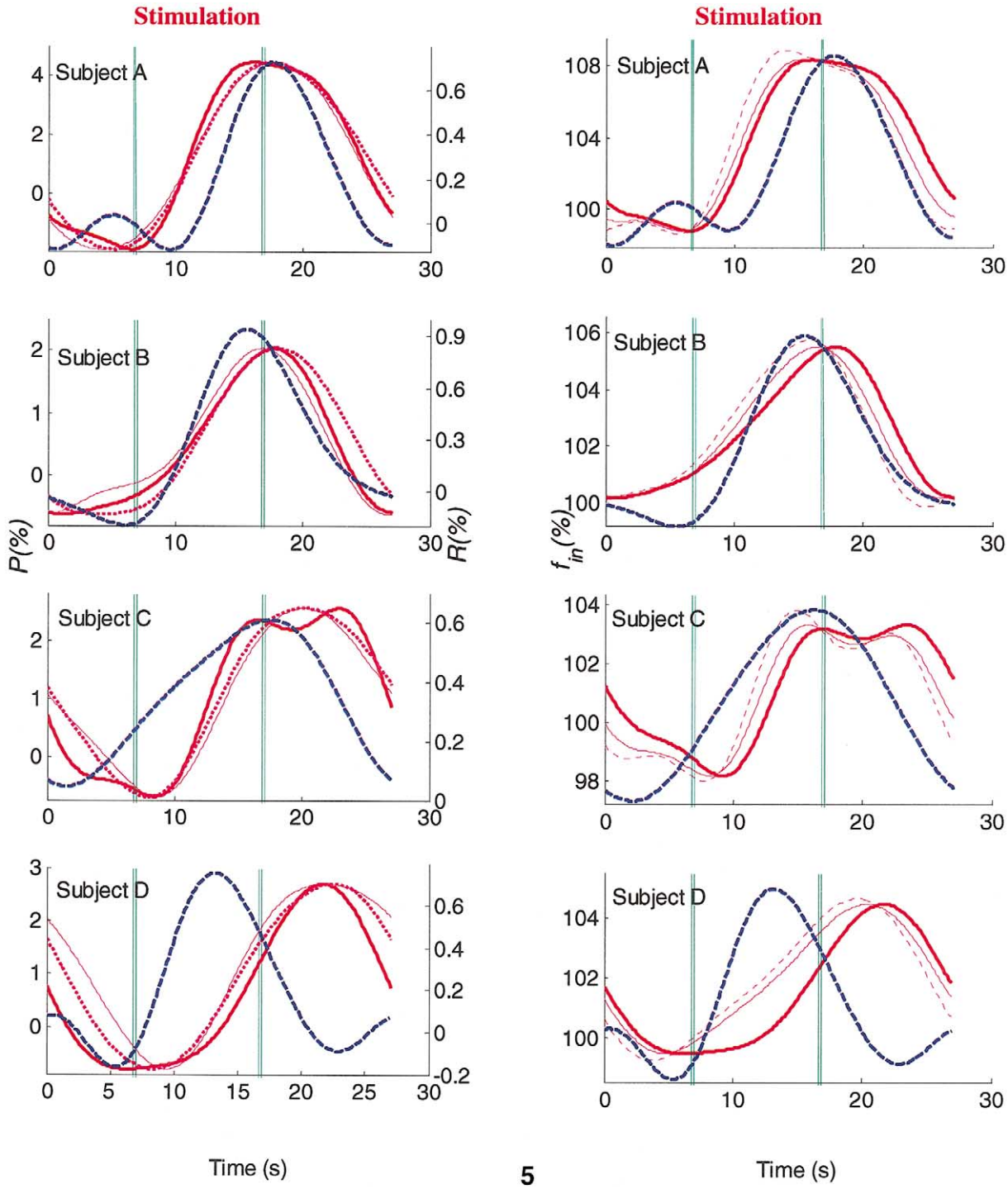

Fig. 4. Changes in P (solid lines), R (dashed lines), and the BOLD signal (dotted lines). The BOLD signals are scaled to the range of P. Vertical marks indicate the beginning and end of stimulation. The zero level on the vertical axes corresponds to the baseline before the beginning of the exercise.

Fig. 5. Time course of P (bold solid lines), R (bold dashed lines), and f_{in} (solid and dashed hairlines). The vertical axis shows the values of f_{in} in percent; f_{in} = 100% corresponds to the baseline level. The P and R signals are scaled to the range of f_{in}. Solid and dashed hairlines correspond to f_{in} obtained at τ_0 = 1 s and τ_0 = 2 s, respectively.

a statistically significant change with a confidence level of 95%. The Bonferroni correction was applied to reduce the probability of assigning spurious activation. This analysis was performed by using the MEDx 3.4 software package (Sensor Systems, Inc., Sterling, VA).

The bulk baseline optical properties, $\mu_a(758)$, $\mu_a(830)$, $\mu_s'(758)$, and $\mu_s'(830)$, of the head tissue at 758 nm and 830 nm, were obtained by fitting the slopes of the calibrated phase and the logarithm of the AC of the optical signals, measured at different source-detector distances, to the exact

Table 1
Numerical data obtained from simultaneous NIR and fMRI measurements[a]

Subject	$[O_2Hb]_0$ (μM)	$[HHb]_0$ (μM)	$\Delta[O_2Hb]$ (μM)	$\Delta[HHb]$ (μM)	ΔP%	C_P	ΔR%	C_R	A_P/A_R	r^2 with R	r^2 without R
A	40.5 ± 4.6	18.9 ± 2.9	1.62	1.20	6.33	0.99	0.84	0.89	2.40 ± 1.15	0.985	0.983
B	30.1 ± 2.8	6.0 ± 1.7	0.50	0.21	3.50	0.98	0.91	0.95	2.84 ± 0.52	0.975	0.9665
C	40.1 ± 5.1	6.2 ± 1.2	0.41	0.22	3.58	0.94	0.55	0.44	2.18 ± 1.63	0.9093	0.8908
D	32.2 ± 3.4	12.8 ± 1.6	0.41	0.38	3.45	0.91	0.83	−0.33	3.61 ± 0.95	0.8661	0.8447

[a] Column 1, subject identification; columns 2–3, baseline values of oxy- and deoxyhemoglobin concentrations; columns 4–5, magnitudes of changes in $[O_2Hb]$ and [HHb] between the maximum and minimum values; column 6, magnitude of change in P (between maximum and minimum in % of baseline [HHb]); column 7, correlation coefficient between changes in P and the BOLD signal; column 8, magnitude of the change in R (between maximum and minimum in % of baseline $[O_2Hb]$); column 9, correlation coefficient between changes in R and the BOLD signal; column 10, ratio of the coefficients A_P and A_R, columns 11 and 12, values of r^2 statistic for the linear regression fit of the BOLD signal using both P and R (column 11) and P only (column 12). NIR, near infrared; fMRI, functional magnetic resonance imaging; BOLD, blood oxygen level dependent.

analytical solution of the light diffusion equation. The method is described in detail in the study by Fantini et al. (1995). The calibration values were obtained from the measurements on the silicone phantom using the same sensor. The values of $[O_2Hb]$ and [HHb] and their changes were obtained by using the spectroscopic relationship between the absorption coefficients of the medium and the concentrations of the chromophores:

$$[O_2Hb] = \frac{\mu_a^{\lambda 1}\,\varepsilon_{Hb}^{\lambda 2} - \mu_a^{\lambda 2}\,\varepsilon_{Hb}^{\lambda 1}}{\varepsilon_{HbO_2}^{\lambda 1}\,\varepsilon_{Hb}^{\lambda 2} - \varepsilon_{Hb}^{\lambda 1}\,\varepsilon_{HbO_2}^{\lambda 2}} \tag{6}$$

$$[HHb] = \frac{\mu_a^{\lambda 2}\,\varepsilon_{HbO_2}^{\lambda 1} - \mu_a^{\lambda 1}\,\varepsilon_{HbO_2}^{\lambda 2}}{\varepsilon_{HbO_2}^{\lambda 1}\,\varepsilon_{Hb}^{\lambda 2} - \varepsilon_{Hb}^{\lambda 1}\,\varepsilon_{HbO_2}^{\lambda 2}} \tag{7}$$

where $\lambda_1 = 758$ nm, $\lambda_2 = 830$ nm, and $\varepsilon^{\lambda}_{[O_2Hb]}$ and $\varepsilon^{\lambda}_{[HHb]}$ [$\mu M^{-1}cm^{-1}$] are the extinction coefficients of oxy- and deoxyhemoglobin, respectively. The on-line conversion of the optical data into the hemodynamic signals was performed by using the software BOXY (ISS). Most of the off-line time series processing was performed by using MATLAB (Version 6.0.0.88, Release 12).

The baseline values $[O_2Hb]_0$ and $[HHb]_0$ were obtained by averaging the time series over their entire lengths. The time series were detrended by using a third order polynomial fit and smoothed by using a low-pass filter with a cutoff frequency corresponding to a time period of 10 s. To further increase the S/N in the measured changes $[HHb]_0 - [HHb]$ and $[tHb]_0 - [tHb]$ (denoted as $\Delta[O_2Hb]$ and $\Delta[HHb]$, respectively) a time-locked averaging of the traces related to 10 stimulation-relaxation cycles was performed. The time-locked averaging returned the averaged $\Delta[O_2Hb]$ and $\Delta[HHb]$ traces consisting of 170 data points per cycle with a temporal resolution of 160 ms.

Polynomial detrending, low-pass filtering, and time-locked averaging were applied to the fMRI data. Since the TR for the EPI images was 1280 ms (a temporal resolution eight times longer than for the NIR data), time-locked folding returned a set of 22 images per stimulation cycle. The resulting averaged sets of EPI images corresponding to the stimulation/relaxation cycle were analyzed by bivariate regression analysis using the averaged traces with $R(t) = \Delta[O_2Hb]/[O_2Hb]_0$ and $P(t) = -\Delta[HHb]/[HHb]_0$ as the regressors. From this analysis the values of the regression F and r^2 statistics were computed for each voxel. The voxel was considered as "activated" if its F value was higher than the 99.9% percentile of the total distribution of F values. (Most of these voxels were identical to the activated voxels revealed by the t test comparison between stimulation and rest.) The BOLD signals of the activated voxels were averaged, normalized to the mean value of the EPI voxel intensity, S_0, and again subjected to bivariate regression analysis using the linear model

$$\frac{\Delta S(t)}{S_0} = A_P P(t) + A_R R(t) + \varepsilon \tag{8}$$

where $\Delta S(t)$ is the average BOLD signal, A_P and A_R are constants, and ε is the residual. In a further analysis, the time-locked and volume-averaged signals from the activated voxels determined by using a t test were also used as the parameter $\Delta S(t)$. To obtain f_{in} and f_{out}, $q(t) = 1 - P(t)$ and $v(t) = 1 + R(t)$ were substituted into the system of Eqs. (2) and (3) with $E(f_{in})$ given in Eq. (4) and then solved numerically to give the values of f_{in} and f_{out}.

Results

Measurements were performed on four healthy right-handed male hairless volunteers, 18 to 57 years old. Informed consent was obtained from all subjects. These subjects are identified as A, B, C, and D.

Fig. 2 shows averaged $\Delta[O_2Hb]$ and $\Delta[HHb]$ traces corresponding to one stimulation-relaxation period for all four subjects. One can see that in all subjects the deoxyhemoglobin concentration decreased during stimulation, while the oxyhemoglobin concentration increased. By comparing the magnitudes of changes in the $\Delta[O_2Hb]$ and $\Delta[HHb]$ (see also Table 1) one can see that the ratio was between 1 and 2.5 for all subjects. The oxygenation of tissue is typically higher than 60% (Elwell et al., 1994), and this indicated that the relative change in total hemoglobin $\Delta[tHb] = \Delta[O_2Hb]$

+ Δ[HHb] was significantly smaller than the relative change in [HHb].

Fig. 3 shows a typical *F*-statistic map obtained from bivariate regression analysis of the BOLD signal using regressors $P(t) = -\Delta[\mathrm{HHb}]/\mathrm{HHb}_0$ and $R(t) = \Delta[t\mathrm{Hb}]/[t\mathrm{Hb}]_0$. The highest values of the regression *F* statistic correspond to the voxels situated in the left primary motor area near the central sulcus. The position of the radiological marker indicated that the center of the optical sensor was reasonably close to the voxels showing the highest *F* values (about 20–25 mm distance). The number of activated voxels, i.e., the voxels with *F* values higher than the 99.9% percentile in subjects B, C, and D was equal to 20 in each case. In Subject A the activated area was somewhat larger (33 voxels) and closer to the optical sensor than in the others (about 15 mm distance). This correlated with the significantly larger magnitude of the hemodynamic changes observed in Subject A than in the other subjects.

Fig. 4 shows averaged traces for the variables *P* and *R*, and the BOLD signal. The dotted curves show the averaged BOLD signals from the activated voxels determined by using regression with *P* and *R*, and the hairline curves show the BOLD signals from the activated voxels determined by using the *t* test. One can see that both methods gave similar curves (the BOLD signals have been scaled to the range of the variable *P* for each graph). In all panels of Fig. 4 one can see that temporal variations in *R* were correlated with the BOLD signal to a much lower degree than variations in *P*, whose time course was very close to the time course of the BOLD signal. By comparing Figs. 2 and 4, one can see that, although for all subjects the variable *R* exhibited an increase during activation, the time course of *R* (see Fig. 4) was different from the time course of $\Delta[\mathrm{O_2Hb}]$ (see Fig. 2) since the time courses of the $\Delta[\mathrm{O_2Hb}]$ traces and Δ[HHb] traces are themselves shifted with respect to each other.

Table 1 summarizes the numerical data. From Table 1 one can see that the correlation coefficient between the value of *P* and the BOLD signal in all measurements was close to unity, in accordance with the high covariance between *P* and the BOLD signals seen in Fig. 4. The values of the correlation coefficient between *R* and the BOLD signal were significantly smaller. For Subject C they were even negative. The ratio of regression coefficients A_P and A_R was always positive, thus indicating that an increase in the blood volume correlates with an increase in the BOLD contrast. However, the values of the r^2 statistic for the regression only increased slightly when the blood volume changes were included in the regression model. This shows that the contribution of blood volume changes to the BOLD signal was very small compared to the contribution of the deoxyhemoglobin changes. This conclusion is also supported by the fact that the changes in *R* were significantly smaller than changes in *P* (comparing columns 6 and 8 of Table 1). The values in Table 1 related to the BOLD signals are shown for signals from activated voxels determined by using the *t* test. In the case of signals from voxels determined using regression with the variables *P* and *R*, the values were very close to those presented in Table 1.

The NIRS data were then incorporated into the balloon model to investigate changes in the parameters rCBV, f_{in}, and f_{out}. The values of E_0 and τ_0 were chosen close to those suggested in the study by Buxton et al. (1998), i.e., $E_0 = 0.4$ and $\tau_0 = 2$ s (to investigate further the role of τ_0, this parameter was varied between 1 and 3 s). In all subjects the time course of deoxyhemoglobin signals closely followed the changes in f_{in} (Fig. 5). In contrast to the deoxyhemoglobin concentration, the time course of the blood volume did not exhibit significant correlation with changes in the blood flow (Fig. 5). An increase in the value of τ_0 resulted primarily in the longer delay between *P* and f_{in}. The delay was approximately equal to τ_0 for all subjects. Analyzing the time course of f_{in} and f_{out} in the balloon model, it was found that for all subjects the difference between f_{in} and f_{out} was much smaller than the range of changes in both values (Fig. 6).

The temporal behavior of the OEF [using Eq. (4)] and $\mathrm{CMRO_2}$ [which is proportional to the product of $E(t)$ and $f_{in}(t)$] was also studied. It was found that while *E* decreased during stimulation by about 2% of its baseline value, the $\mathrm{CMRO_2}$ exhibited elevation of about 1% (Fig. 7). This $\mathrm{CMRO_2}$ increase was synchronous with the increase in the flow. Thus, changes in the [HHb] and BOLD signals followed $\mathrm{CMRO_2}$ changes, with a delay approximately equal to τ_0.

Discussion

The results of our analysis of the fMRI data are in the qualitative agreement with Buxton's model of the BOLD signal as a function of deoxyhemoglobin concentration and rCBV (Buxton et al., 1998). Indeed, the positive values of $A_\mathrm{P}/A_\mathrm{R}$ obtained in this study indicate that an increase in the blood volume correlates with an increase in the BOLD signal, as does the decrease in [HHb]. At a magnetic field strength of 1.5 T, and using a TE of 40 ms, the values of the parameters k_1, k_2, and k_3 are approximately 2.8, 0.57, and 0.43, respectively (Hess at al., 2000). Therefore the values of $A_\mathrm{P}/A_\mathrm{R}$ obtained here are in a relatively good quantitative agreement with the ratio $(k_1 + k_2)/(k_2 + k_3) = 3.37$. However, the stepwise regression analysis showed that the overall contribution of the blood volume changes to the BOLD signal were qualitatively negligible compared to the contribution of Δ[HHb]. One should note that this conclusion is the result of multiple regression and correlation analyses methods, which both exclusively depend upon the shapes of the curves, but not the absolute amplitudes, so that extremely accurate calibration of signals is not necessary. The small contribution of the rCBV to the BOLD signal can be explained by the fact that the relative changes in $[\mathrm{O_2Hb}]$ and $[t\mathrm{Hb}]$ (represented by the variable $R = \Delta[t\mathrm{Hb}]/[t\mathrm{Hb}]_0$) during functional activation were much smaller than the rela-

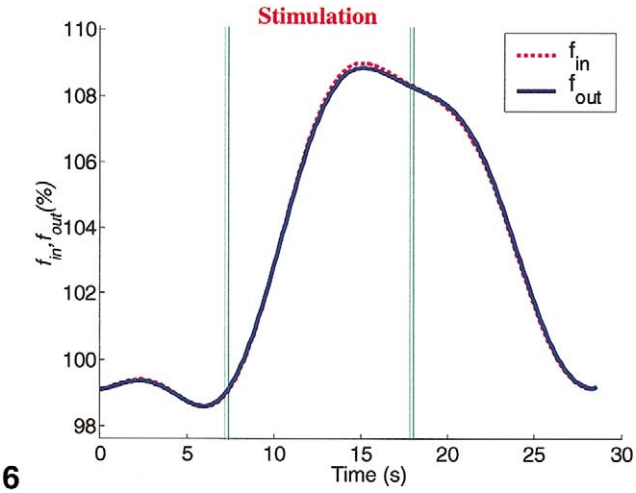

6

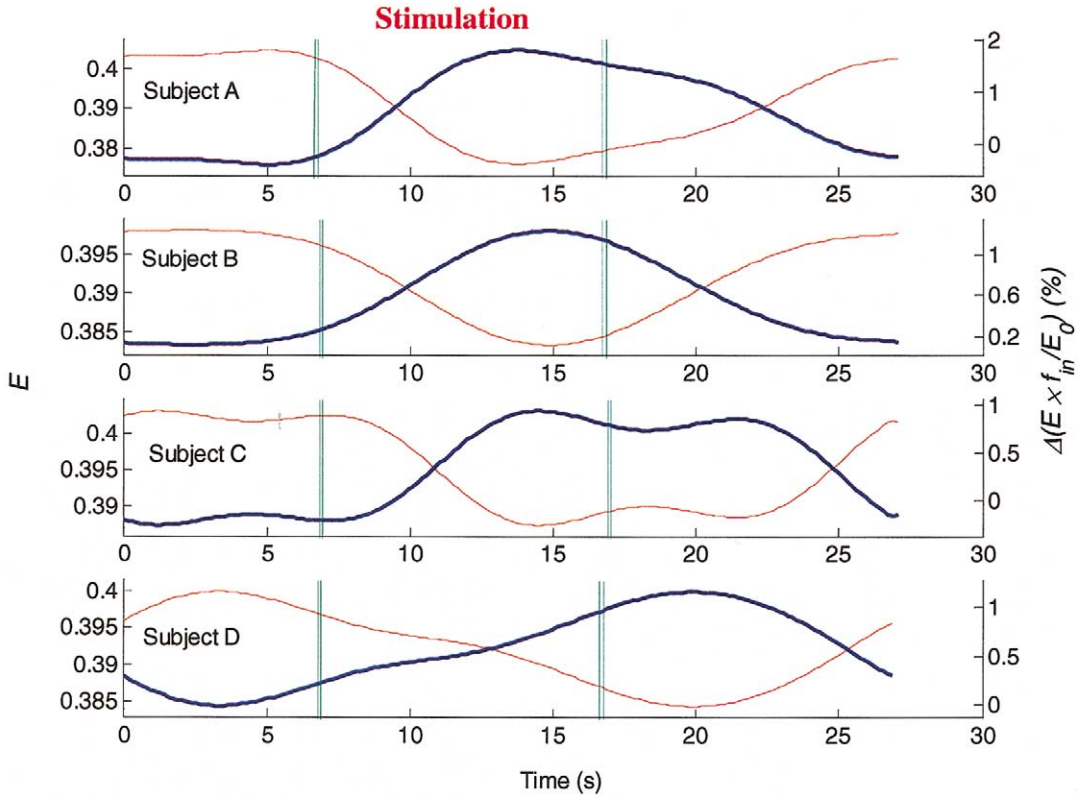

7

Fig. 6. Time course of f_{in} and f_{out} for Subject A. $E_0 = 0.4$ and $\tau_0 = 2$ s.
Fig. 7. Changes in $E(t)$ and $E(t) \times f(t)$ (which is proportional to $CMRO_2$) at $E_0 = 0.4$ and $\tau_0 = 2$ s.

tive change in $P = -\Delta[\mathrm{HHb}]/[\mathrm{HHb}]_0$. Thus, one can conclude that the BOLD signal observed during motor activation in humans is, by and large, a measure of the cerebral deoxyhemoglobin concentration changes. This result agrees with the previous observation by Kleinschmidt et al. (1996) that total hemoglobin does not show changes consistent with the fMRI signal. However, the observed high correlation between BOLD and deoxyhemoglobin concentration changes is in contradiction with the results of Strangman et al. (2002), who found highly variable correlations for different subjects. One possible explanation for these highly variable correlations obtained by Strangman et al. (2002) were due to the near-infrared technique used in their study, which was a single source-detector method. Previously our group also used this technique (Toronov et al., 2001), and found that it is highly sensitive to superficial hemodynamic fluctuations in the scalp. These fluctuations bias the signals, thus reducing the correlation with the BOLD signal. This was the main reason to choose the multidistance technique used in the current investigation.

One should stress that the small magnitude of the change in R is due to the following two factors: (1) the similarity of

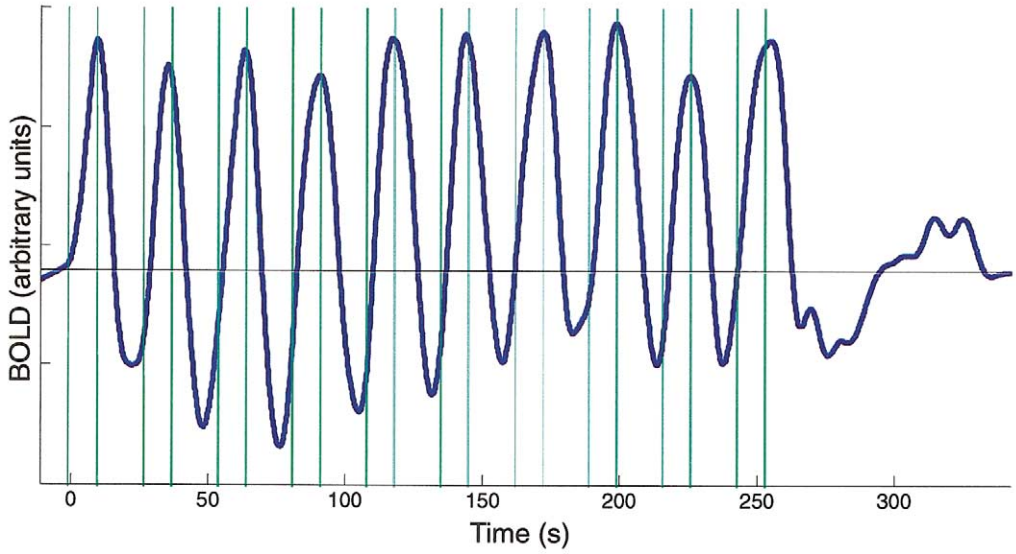

Fig. 8. The BOLD signal corresponding to 10 activation trials in Subject A without time-locked averaging. The horizontal line shows the baseline signal before the exercise.

the magnitudes of $\Delta[O_2Hb]$ and $\Delta[HHb]$, which change in opposite directions, and (2) the high oxygen saturation of cerebral blood. It is important to consider possible artifacts that could affect these two factors. The values of $[O_2Hb]_0$ and $[HHb]_0$ shown in Table 1 correspond to a total rCBV of 3–3.5 mg per 100 g of tissue. These values are in a good agreement with those measured using PET (Ito et al., 2001), and by other groups using NIRS (Elwell et al., 1994). This is a strong indication that these values have been determined without significant errors. However, the method of measurement of the optical properties used here assumes homogeneity of the medium. Since functional hemodynamic changes occur only in a small region of the brain, the method can underestimate the magnitudes of the localized changes in cerebral $[O_2Hb]$ and [HHb]. However, the correction factors necessary to account for such errors should be the very similar for both $\Delta[O_2Hb]$ and $\Delta[HHb]$. Therefore, this artifact should not affect the ratio of the magnitudes of the changes in P and R.

The small relative changes in the measured rCBV, compared to the relative changes in deoxyhemoglobin concentration, and the fact that the time course of the total hemoglobin concentration is different from that of oxyhemoglobin, indicates that the underlying physiological mechanism of the BOLD effect is the "washout" of deoxyhemoglobin by an increased blood flow, rather than the dilution of HHb in the increased volume of blood that flows to the activated region. This mechanism is in agreement with application of the balloon model to our data, in that during activation the decrease in [HHb] followed almost perfectly the increase in rCBF, while the rCBV did not exhibit significant correlation with the rCBF. Thus, according to the balloon model, the BOLD signal follows changes in rCBF with a delay approximately equal to V_0/F_0.

Although our results do not contradict the basic assumptions of the balloon model (Buxton et al., 1998), the small increase of the rCBV during the functional activation indicates that there is no appreciable balloon effect per se. This leads to simplification of the system of Eqs. (2) and (3). Indeed, since the changes in $v = 1 + R$ are small, to describe the BOLD signal one can use Eq. (2) alone, with the value of $v \approx 1$. Also, instead of modeling f_{out} as a function of v as in the studies by Buxton et al. (1998) and Feng et al. (2001), one can assume that $f_{out} \approx f_{in} = f$. Then, the system reduces to only one equation:

$$\frac{dq}{dt} = \frac{1}{\tau_0}\left[\frac{E(f)}{E_0} - q(t)\right] f(t) \tag{9}$$

where $f(t)$ is the flow through the activated region, and $E(f)$ is given by Eq. (4). Since the BOLD signal reflects changes in $q(t)$, the independent variables $q(t)$ and $f(t)$ in the Eq. (9) could both be measured by a combined BOLD and ASL protocol.

One should emphasize that there is no discrepancy between our results and those of Buxton et al. (1998) in that the shapes of the negative of deoxyhemoglobin concentration changes and the BOLD signal are similar. However, our data suggest different dynamic roles of the rCBV and rCBF, and in particular a different interpretation of the poststimulus undershoot in the BOLD signal. In Fig. 4, several seconds before the beginning of stimulation, plots of $P(t)$ and the BOLD signal are at levels below the baseline at the beginning of the study. This feature of the BOLD signal is known as the poststimulus undershoot, which corresponds to an overshoot in the deoxyhemoglobin concentration (Buxton et al, 1998). Buxton et al. (1998) interpreted this feature using the balloon model of Eqs. (2)–(4), arguing

that there was no undershoot in rCBF, but the overshoot in the deoxyhemoglobin content and undershoot in the BOLD signal resulted from the slow return of the rCBV to its baseline value. Our data suggest that, since the rCBV changes very little and inconsistently with the BOLD signal, the reason for the poststimulus overshoot in the deoxyhemoglobin concentration is in fact a corresponding undershoot in the rCBF. To further clarify this issue, the BOLD signal corresponding to 10 activation trials in Subject A without time-locked averaging is shown in Fig. 8. Although the timing of the rest periods (17 s) was shorter than necessary (30–40 s) for the BOLD signal to return completely to its baseline level one can clearly see the poststimulus undershoots. It is also important to note that at each later stimulation period the shape of the signal is approximately the same as during the first one. An important question is whether the short rest period suppresses the contribution of changes in rCBV to the BOLD signal undershoot. If changes in the rCBV play an important role in the undershoot of the BOLD signal, and if there were significant suppression of this effect due to the interstimulus interval, one would expect that the magnitude of the BOLD undershoot would decrease over the 10 stimulation periods. In fact, Fig. 8 shows that there is no decrease in the magnitude of the BOLD undershoot signal. If the undershoot were due to a slower return to the baseline in the rCBV than in the rCBF and deoxyhemoglobin content, then after the first one or two stimuli the balloon would be almost fully inflated, the rCBV would not change between stimulation and rest periods, and changes in the BOLD signal could be attributed solely to the changes in rCBF. If the rCBV were "frozen" at this high level, the only explanation for the undershoot in the BOLD signal would be that the rCBF also undergoes an undershoot. Such an undershoot is indeed seen in the flow curves for subjects A, C, and D in Fig. 5, where the 100% level of f_{in} corresponds to the baseline before the beginning of the exercise.

Conclusion

Our results have shown that, at 1.5 T, the change in deoxyhemoglobin concentration is the major factor determining the time course of the BOLD signal in the human motor cortex during motor stimulation. The influence of changes in rCBV is qualitatively in agreement with recently established theories, but is much smaller than that of changes in the deoxyhemoglobin concentration. The increase in cerebral blood oxygenation during functional activation is due to an increase in the rCBF velocity, and occurs without a significant swelling of the blood vessels. The BOLD signal follows changes in rCBF with a time delay approximately equal to the ratio of the baseline values of the rCBV and rCBF. The relationship between the BOLD signal and rCBF can be quantified using a simple equation [Eq. (9)].

Acknowledgments

This study was supported by National Institutes of Health (NIH) grants DA14111, CA57032, and RR10966.

References

Bandettini, P.A., Kwong, K.K., Davis, T.L., Tootell, R.B., Wong, E.C., Fox, P.T., Belliveau, J.W., Weisskoff, R.M., Rosen, B.R., 1997. Characterization of cerebral blood oxygenation and flow changes during prolonged brain activation. Hum. Brain Mapp. 5, 93–109.

Belliveau, J.W., Kennedy Jr., D.N., McKinstry, R.C., Buchbinder, B.R., Weisskoff, R.M., Cohen, M.S., Vevea, J.M., Brady, T.J., Rosen, B.R., 1991. Functional mapping of the human visual cortex by magnetic resonance imaging. Science 254, 716–719.

Benaron, D.A., Stevenson, D.K., 1994. Resolution of near infrared time-of-flight brain oxygenation imaging. Adv. Exp. Med. Biol. 345, 609–617.

Boxerman, J.L., Bandettini, P.A., Kwong, K.K., Baker, J.R., Davis, T.L., Rosen, B.R., Weisskoff, R.M., 1995. The intravascular contribution to fMRI signal change: Monte Carlo modeling and diffusion-weighted studies in vivo. Magn. Reson. Med. 34, 4–10.

Buxton, R.B., Frank, L.R., 1997. A model for the coupling between cerebral blood flow and oxygen metabolism during neural stimulation. J. Cereb. Blood Flow Metab. 17, 64–72.

Buxton, R.B., Wong, E.C., Frank, L.R., 1998. Dynamics of blood flow and oxygenation changes during brain activation: the balloon model. Magn. Reson. Med. 39, 855–864.

Chance, B., Zhuang, Z., Unah, C., Alter, C., Lipton, L., 1993. Cognition-activated low-frequency modulation of light absorption in human brain. Proc. Natl. Acad. Sci. USA 90, 3770–3774.

Colier, W.N., Quaresima, V., Oeseburg, B., Ferrari, M., 1999. Human motor-cortex oxygenation changes induced by cyclic coupled movements of hand and foot. Exp. Brain Res. 129, 457–461.

Elwell, C.E., Cope, M., Edwards, A.D., Wyatt, J.S., Delpy, D.T., Reynolds, E.O., 1994. Quantification of adult cerebral hemodynamics by near-infrared spectroscopy. J. Appl. Physiol. 77, 2753–2760.

Fantini, S., Franceschini, M.A., Maier, J.S., Walker, S.A., Barbieri, B., Gratton, E., 1995. Frequency-domain multichannel optical detector for noninvasive tissue spectroscopy and oximetry. Opt. Eng. 34, 32–42.

Feng, C.M., Liu, H.L., Fox, P.T., Gao, J.H., 2001. Comparison of the experimental BOLD signal change in event-related fMRI with the balloon model. NMR Biomed. 14, 397–401.

Ferrari, M., Wilson, D.A., Hanley, D.F., Traystman, R.J., 1992. Effects of graded hypotension on cerebral blood flow, blood volume, and mean transit time in dogs. Am. J. Physiol. 262, H1908–H1914.

Ferrari, M., Zanette, E., Giannini, I., Sideri, G., Fieschi, C., Carpi, A., 1986. Effects of carotid artery compression test on regional cerebral blood volume, hemoglobin oxygen saturation and cytochrome-C-oxidase redox level in cerebrovascular patients. Adv. Exp. Med. Biol. 200, 213–221.

Ferrari, M., Zanette, E., Sideri, G., Giannini, I., Fieschi, C., Carpi, A., 1987. Effects of carotid compression, as assessed by near infrared spectroscopy, upon cerebral blood volume and hemoglobin oxygen saturation. J. R. Soc. Med. 80, 83–87.

Fox, P.T., Mintun, M.A., Raichle, M.E., Miezin, F.M., Allman, J.M., Van Essen, D.C., 1986. Mapping human visual cortex with positron emission tomography. Nature 323, 806–809.

Franceschini, M.A., Toronov, V., Filiaci, M., Gratton, E., Fantini, S., 2000. On-line optical imaging of the human brain with 160-ms temporal resolution. Optics Express 6, 49–57.

Hess, A., Stiller, D., Kaulisch, T., Heil, P., Scheich, H., 2000. New insights into the hemodynamic blood oxygenation level-dependent response through combination of functional magnetic resonance imaging and optical recording in gerbil barrel cortex. J. Neurosci. 20, 3328–3338.

Hirth, C., Obrig, H., Valdueza, J., Dirnagl, U., Villringer, A., 1997. Simultaneous assessment of cerebral oxygenation and hemodynamics during a motor task. A combined near infrared and transcranial Doppler sonography study. Adv. Exp. Med. Biol. 411, 461–469.

Ito, H., Kanno, I., Iida, H., Hatazawa, J., Shimosegawa, E., Tamura, H., Okudera, T., 2001. Arterial fraction of cerebral blood volume in humans measured by positron emission tomography. Ann. Nucl. Med. 15, 111–116.

Kato, T., Kamei, A., Takashima, S., Ozaki, T., 1993. Human visual cortical function during photic stimulation monitoring by means of near-infrared spectroscopy. J. Cereb. Blood Flow Metab. 13, 516–520.

Kleinschmidt, A., Obrig, H., Requardt, M., Merbodt, K.D., Dirnagl, U., Villringer, A., Frahn, J., 1996. Simultaneous recording of cerebral blood oxygenation changes during human brain activation by magnetic resonance imaging and near-infrared spectroscopy. J. Cereb. Blood Flow Metab. 16, 817–826.

Obrig, H., Wenzel, R., Kohl, M., Horst, S., Wobst, P., Steinbrink, J., Thomas, F., Villringer, A., 2000. Near-infrared spectroscopy: does it function in functional activation studies of the adult brain? Int. J. Psychophysiol. 35, 125–142.

Ogawa, S., Menon, R.S., Tank, D.W., Kim, S.G., Merkle, H., Ellermann, J.M., Ugurbil, K., 1993. Functional brain mapping by blood oxygenation level-dependent contrast magnetic resonance imaging. A comparison of signal characteristics with a biophysical model. Biophys. J. 64, 803–812.

Ruben, J., Wenzel, R., Obrig, H., Villringer, K., Bernarding, J., Hirth, C., Heekeren, H., Dirnagl, U., Villringer, A., 1997. Haemoglobin oxygenation changes during visual stimulation in the occipital cortex. Adv. Exp. Med. Biol. 428, 181–187.

Sakatani, K., Chen, S., Lichty, W., Zuo, H., Wang, Y.P., 1999. Cerebral blood oxygenation changes induced by auditory stimulation in newborn infants. Early Hum. Dev. 55, 229–236.

Strangeman, G., Culver, J.P., Thompson, J.H., Boas, D.A., 2002. A quantitative comparison of simultaneous Bold fMRI and NIRS recordings during functional brain activation. NeuroImage 17, 719–731.

Toronov, V., Franceschini, M.A., Filiaci, M., Fantini, S., Wolf, M., Michalos, A., Gratton, E., 2000. Near-infrared study of fluctuations in cerebral hemodynamics during rest and motor stimulation: temporal analysis and spatial mapping. Med. Phys. 27, 801–815.

Toronov, V., Webb, A., Choi, J.H., Wolf, M., Michalos, A., Gratton, E., Hueber, D., 2001. Investigation of human brain hemodynamics by simultaneous near-infrared spectroscopy and functional magnetic resonance imaging. Med. Phys. J. 28, 521–527.

Ugurbil, K., Adriany, G., Andersen, P., Chen, W., Gruetter, R., Hu, X., Merkle, H., Kim, D.S., Kim, S.G., Strupp, J., Zhu, X.H., Ogawa, S., 2000. Magnetic resonance studies of brain function and neurochemistry. Annu. Rev. Biomed. Eng. 2, 633–660.

Vanzetta, I., Grinvald, A., 1999. Increased cortical oxidative metabolism due to sensory stimulation: implications for functional brain imaging. Science 286, 1555–1558.

Villringer, A., Chance, B., 1997. Non-invasive optical spectroscopy and imaging of human brain function. Trends Neurosci. 20, 435–442.

Villringer, A., Planck, J., Hock, C., Schleinkofer, L., Dirnagl, U., 1993. Near infrared spectroscopy (NIRS): a new tool to study hemodynamic changes during activation of brain function in human adults. Neurosci. Lett. 154, 101–104.